Study of Current Third-Order Harmonics Control to Reduce Iron Loss in Permanent Magnet Synchronous Motors

Kaiki Akizuki, Toshiyuki Fujita,
and Hiroshi Fujimoto
The University of Tokyo
Kashiwa, Chiba, Japan
akizuki.kaiki22@ae.k.u-tokyo.ac.jp

Michihiro Nakagawa, Naoya Yamashita,
Takayuki Miyajima, Yoshiki Yasuda,
and Akio Yamagiwa
DAIKIN INDUSTRIES, Ltd
Settsu, Osaka, Japan

***Abstract*—Permanent magnet synchronous motors (PMSMs) are widely used for their advantages. Considering the expansion of applications and long-term operation as industrial equipment, achieving further high-efficiency driving is required for environmental impact reduction. One of the factors that affects iron loss is current harmonics. This paper investigates an appropriate injection control of unbalanced third harmonic currents in order to reduce iron loss in current control for achieving further high-efficiency driving of PMSMs. From the experimental results by H-coil method which can measure directly iron loss in the motor, the iron loss is reduced by the suppression of magnetic field strength peak and magnetic flux density peak compared to the conventional current control methods in the rated-load region.**

***Index Terms*—Permanent magnet synchronous motor(PMSM), Iron loss, Current third-order harmonics injection, H-coil method**

I. Introduction

Permanent magnet synchronous motors (PMSMs) have many advantages such as high output power and high-efficiency driving [1]–[3]. For these reasons, PMSMs are utilized in various fields, including household appliances, electric vehicles [4], industrial machinery, and more.

There are primarily three types of driving losses in PMSMs: copper loss due to the resistance of the windings, iron loss occurring in the core and magnet, and mechanical loss resulting from rotational friction. In PMSMs, it is important to reduce the iron loss for achieving higher-efficiency driving because the magnetic flux density in the iron core is high and the iron loss generated in the magnet and iron core is dominant.

Various types of control method on PMSM have been studied [5], [6] and there are many studies on loss reduction control methods. Maximum Torque Per Ampere (MTPA) control are well known for reducing copper loss [7]. However, this method did not necessarily guarantee the most efficient driving because they did not consider iron loss. Other approaches related to reducing iron loss through control were those focusing on PWM waveforms [8], optimization of modulated currents [9], and models based on an extension of conventional equivalent iron loss models [10], and so on [11]–[13]. However, an equivalent iron loss model considering a nonlinearity and the minimization method have not been established yet.

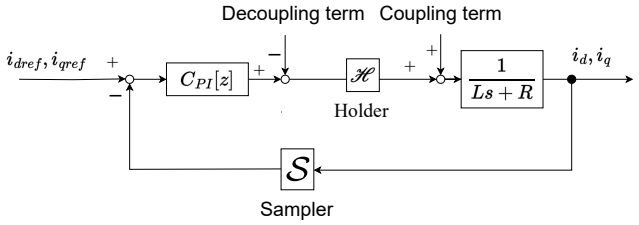

Fig. 1: Block diagram of PI control.

Harmonics affect the performance of PMSMs [14]–[16], and copper loss and iron loss are significantly influenced by them. The authors applied Repetitive Perfect Tracking Control (RPTC) for current control to reduce harmonic-induced iron loss in the input current of PMSM [17]. The effectiveness of this approach was verified through indirect evaluation of iron loss, deducting copper loss and mechanical loss from the input power. Alomost all of previous researches have evaluated iron loss by indirect assessments or simulations. Therefore, it needs to elucidate the mechanism of reducing iron loss.

This paper considers that current peaks in the saturation region are a factor increasing iron loss, an appropriate control method for injecting unbalanced third-order harmonic currents is proposed to suppress current peaks in a 3-phase 3-wire PMSM. Additionally, iron loss is directly measured and evaluated by the H-coil method [18] during this process, and the results are compared with those using conventional current control methods.

II. Conventional methods

A. PI controller

In general, a PI controller is used for current control of PMSM. Fig. 1 shows the block diagram of PI control. The PI controllers are designed by the pole zero cancellation method

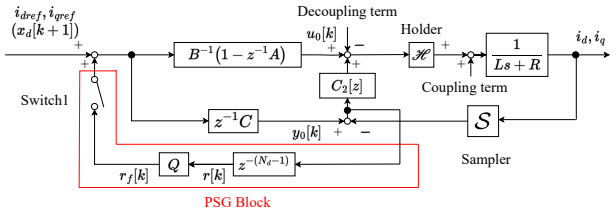

Fig. 2: Block diagram of RPTC.

TABLE I: Parameters for PSG.

Parameter	Meanings
T_d	Fundamental period of disturbance
T_s	Control Period
$r_f[k]$	Output of filter
$r[k]$	Input of filter
γ	Parameter for filter design

and are given as Eq. (1). R is stator winding resistance, L is inductance.

$$C_{PI}(s) = \frac{L_{d(q)}s + R}{\tau s}. \tag{1}$$

B. Repetitive Perfect Tracking Control(RPTC)

Fig. 2 shows the block diagram of RPTC. RPTC consists of PTC [19] and a compensation signal generator based on repetitive control, known as the Periodic Signal Generator (PSG) block. The PSG includes a memory for recording errors aligned with the fundamental period of disturbances, a switch to initiate compensation after reaching a steady state, and a Q filter for sensor noise removal [20]. Table I shows the parameters associated with PSG. The memory aligns the disturbance period with the fundamental wave period as determined by Eq. (2). Additionally, the Q filter in Eq. (3) is a phase-lag-free low-pass filter that requires the value of one sample ahead. By setting γ in Eq. (3), the cutoff frequency is determined, suppressing non-periodic disturbances in RPTC while only suppressing periodic disturbances.

$$N_d = \frac{T_d}{T_s}. \tag{2}$$

$$r_f[k] = \frac{z + \gamma + z^{-1}}{\gamma + 2}. \tag{3}$$

III. Proposed Method

In a three-phase three-wire PMSM, injecting the desired third harmonic currents individually into each phase current is structurally impossible. Therefore, the injection of harmonic currents in the $\alpha\beta$ coordinate system is conducted as follows.

When the fundamental component of the α-axis current is given by Eq. (4), considering a third-order harmonic current with an amplitude of one sixth of the fundamental amplitude and in-phase with the fundamental, as expressed in Eq. (5). Injecting this third-order harmonic current described in Eq. (5), the α-axis current is expressed by Eq. (6). Similar

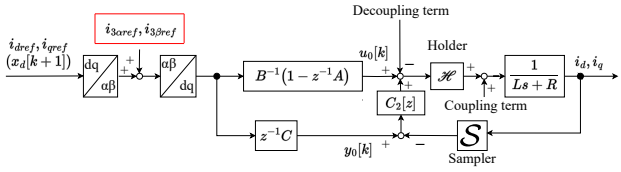

Fig. 3: Unbalanced third-order harmonics injection control(Proposed method).

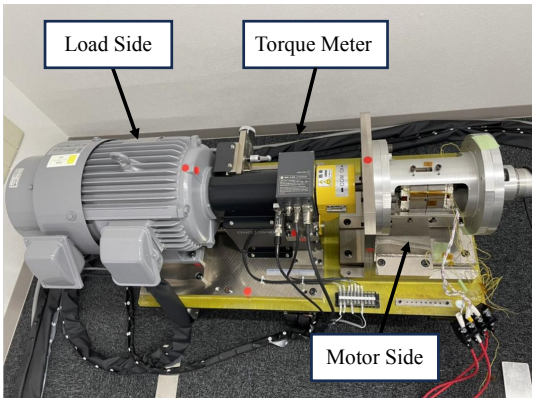

Fig. 4: Experimental setup.

considerations apply to the β-axis current. With the motor currents described in Eq. (6), current peaks are suppressed, and the suppression of magnetic flux saturation is expected in the saturation region.

$$i_{f\alpha ref} = A\sin\omega t. \tag{4}$$

$$i_{3\alpha ref} = \frac{A}{6}\sin 3\omega t. \tag{5}$$

$$i_{\alpha ref} = A\sin\omega t + \frac{A}{6}\sin 3\omega t. \tag{6}$$

Fig. 3 shows the block diagram of proposed method. First, the dq-axis current references are given, which are converted to $\alpha\beta$-axis current references by applying the inverse Park transform to them. Next, third-order harmonic current references are injected to the converted $\alpha\beta$-axis current references based on the policy described in Eq. (5). Finally, $\alpha\beta$-axis current references are converted back to the dq-axis current references

TABLE II: Parameters of experimental IPMSM.

Parameter	Meanings	Value
L_d	d-axis inductance	11.2 mH
L_q	q-axis inductance	21.2 mH
R	Resistance	0.380 Ω
K_e	Permanent magnet flux linkage	0.107 Wb
P	Number of pole pairs	2
$\mathrm{V_{DC}}$	DC voltage	250 V
F_s	Carrier Frequency	10 kHz
T_s	Control Period	0.1 kms
γ	Parameter of filter design	2
τ	Time constant of PI controller	1 ms

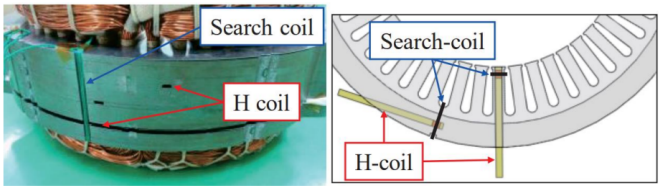

Fig. 5: H-coil method.

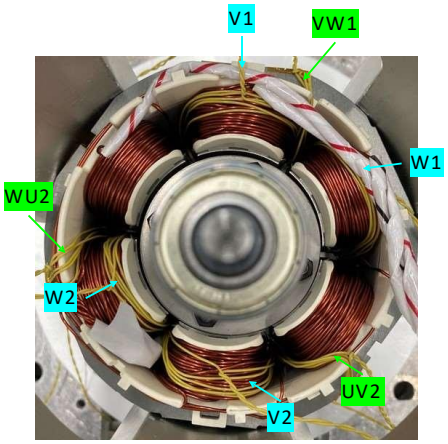

Fig. 6: Measurement points.

by applying the Park transform, and the system is controlled by a perfect tracking control system (PTC) [19].

IV. Experimental Results and Discussion

A. Experimental conditions

Fig. 4 shows the experimental setup and Table II lists the experimental parameters of IPMSM. Setting γ=2 in Eq. (3) results in a cutoff frequency of 1.8 kHz. The rotation speed is set to 3000 rpm (fundamental frequency: 100 Hz) and the dq-axis current references are set to i_d = 0 A and i_q = 6.6 A. Therefore, the third harmonics of $\alpha\beta$-axis current references are 1.1 A. The output torques were constant at 1.41 Nm and DC current ripple due to third-order harmonic injection did not occur when each current control method was applied.

B. Measurement method of BH curve

Fig. 5 shows the image of H-coil method. The magnetic field strength is measured by an H-coil installed in grooves machined into the stator, while the magnetic flux density is measured by a search coil wound directly around a magnetic material. Here, based on the assumption that the magnetic field strength is continuous between inside and just above the magnetic material, the magnetic field strength measured by the H-coil just above the magnetic material can be considered as the magnetic field strength inside the material. Additionally, by winding the search coil near the H-coil, it becomes possible to measure the localized BH loop at positions corresponding to the size of the H-coil.

Fig. 6 shows the measurement points of H-coil method. V1, V2, W1, W2 correspond to the measurements of teeth, while VW1, UV2, and WU2 correspond to the measurements of the back yoke. Due to the fact that iron loss occurring in the teeth is greater compared to that occurring in the back yoke, this paper focuses on the measurement and evaluation of a part of the teeth, namely W1. Since the signal level of the H coil is very small, a high A/D resolution and a high sampling frequency are necessary to measure the terminal voltage with an oscilloscope, especially for measuring the carrier components. Therefore, using the Rohde-Schwarz MXO 4 oscilloscope, which is capable of increasing the A/D resolution up to a maximum of 18 bits and is also compatible with high sampling frequencies. In the measurement, a sampling frequency is set 6.25 MHz, and sample points are set 625,000 points.

TABLE III: Parameters of H-coil and search coil.

Parameter	Meanings	Value
μ_0	Vacuum permeability	$4\pi \times 10^{-7}$ H/m
S_H	H-coil cross-sectional area	3.2×10^{-6} m^2
N_H	Number of H-coil turns	200
S_B	Magnetic cross-sectional area	8.76×10^{-4} m^2
N_B	Number of Search coil turns	5
V	Magnetic volume	1.46×10^{-5} m^3

Table III shows the parameters of H-coil and search coil. The magnetic field strength, magnetic flux density, and iron loss are determined using the induced electromotive e_H generated at both ends of the H-coil and the induced electromotive e_B generated at both ends of the search coil, by the following equations. f is a fundamental frequency of electrical angle.

$$H = \frac{1}{\mu_0 S_H N_H} \int e_H dt. \tag{7}$$

$$B = \frac{1}{S_B N_B} \int e_B dt. \tag{8}$$

$$P = fV \int_0^T H \frac{dB}{dt} dt. \tag{9}$$

C. Experimental results and validity of each current control method

Fig. 7 shows the experimental results of the $\alpha\beta$-axis currents when proposed method was applied. Fig. 7a shows the time waveforms, Fig. 7b shows fourier transform results of of α-axis current, and Fig. 7c shows fourier transform results of of β-axis current. From Fig. 7a, the injection of the third-order harmonic currents suppresseed the peaks of the $\alpha\beta$-axis current waveforms. Fig. 7b and Fig. 7c shows that the measured α-axis current is about 0.10 A larger than the reference of the third-order current harmonic, and the β-axis current is about 0.15 A higher than the reference, resulting in errors of 9.09% and 13.6 % for the α and $beta$ axis currents, respectively. This is due to the modeling errors of inductance L and armature resistance R. Moreover, since this paper does not consider the suppression of the effects of spatial harmonics of the magnet flux and inductance, the 5th-order and 7th-order harmonics were generated in the measured values.

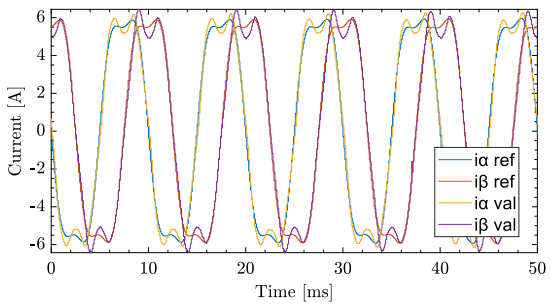

(a)

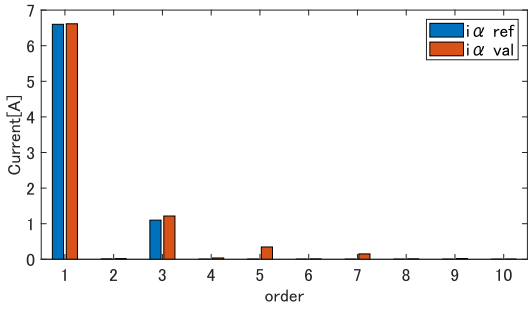

(b)

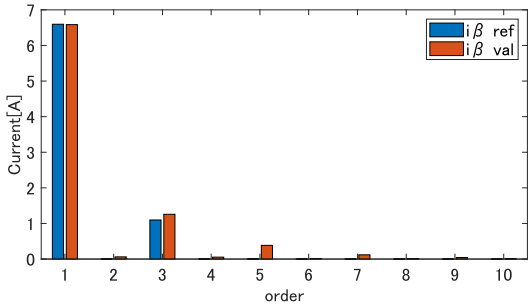

(c)

Fig. 7: Experimental results of propsed method. (a) time waveforms of $\alpha\beta$-axis current. (b) fourier transform results of of α-axis current. (c) fourier transform results of of β-axis current.

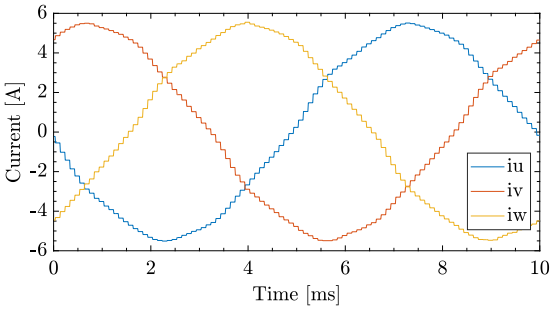

(a)

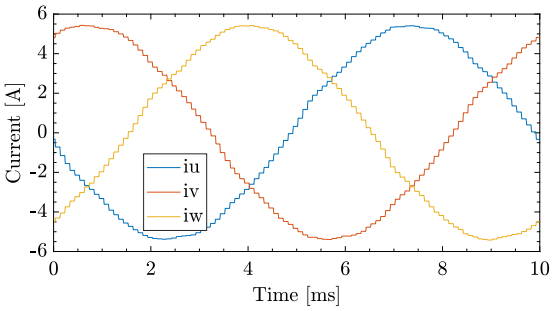

(b)

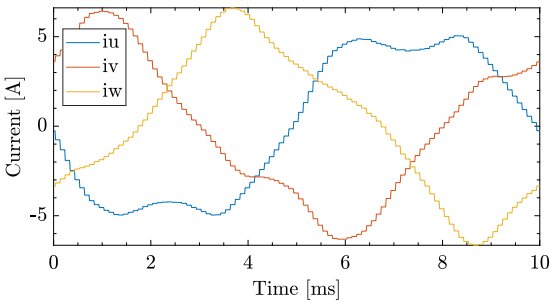

(c)

Fig. 8: Experimental results of 3-phase currents. (a) PI. (b) RPTC. (c) Proposed method.

Fig. 8 shows the experimental results of the 3-phase currents when each current control method was applied. Fig. 8a shows the results of PI control, Fig. 8b shows the results of RPTC, and Fig. 8c shows the results of proposed method. The results in Fig. 8a and Fig. 8b show that the waveform was closer to a sinusoidal waveform in RPTC than in PI control because of the low-order harmonic current suppression control. In Fig. 8c, the $\alpha\beta$ coordinate system was based on the U phase. Furthermore, the time waveform of the 3-phase current references in Fig. 8c shows that it was unbalanced.

D. Iron loss evaluation by BH curve

Fig. 9 shows the measurement results inside the motor when each current control method was applied. Fig. 9a shows the time waveform of magnetic field strength, 9b shows the time waveform of magnetic flux density, and 9c shows the BH curve. The blue color shows the results with PI control, the red color with RPTC applied, and the yellow color with the proposed method applied.

From Fig. 9a the peak of the magnetic field strength waveform was suppressed in accordance with the peak suppression of the current waveform, and was suppressed by 17.3% compared to that in the case of PI control. Similarly, from Fig. 9b the peak of the magnetic flux density waveform was also suppressed, and it was about 8.9% compared to that in the case of PI control. The area of the BH curve is equal to the iron loss value, and the results of Fig. 9c shows that the area of the BH curve is the largest in the case of PI control, then in the case of RPTC, and then in the case of the proposed control, in that order. The iron loss values calculated by Eq. (9) were 0.6420 W/kg for PI control, 0.5013 W/kg for RPTC, and 0.3301 W/kg for the proposed method, as shown in Fig.

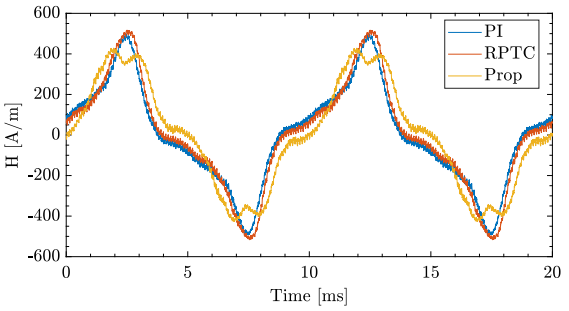

(a)

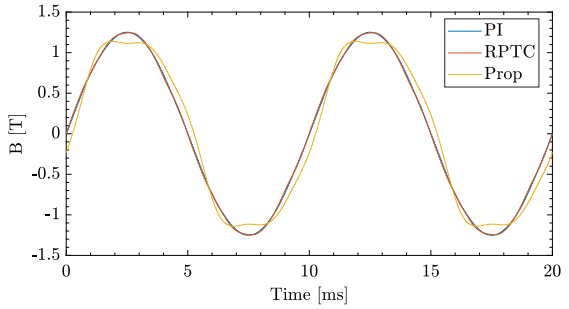

(b)

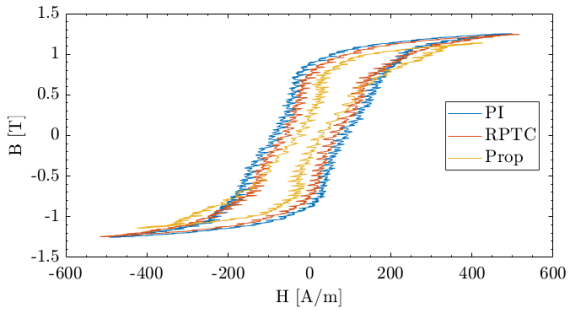

(c)

Fig. 9: Experimental results of magnetic performance during motor drive. (a) measured magnetic field strength waveforms. (b) measured magnetic flux density waveforms. (c) measured BH curves.

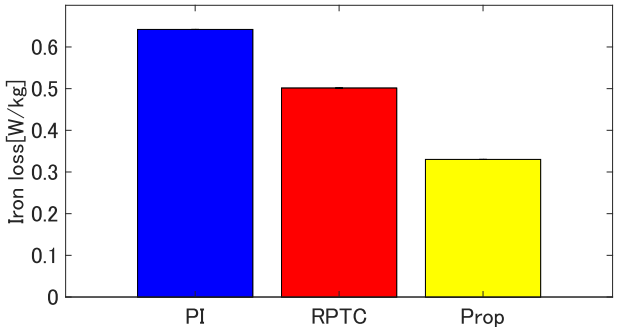

Fig. 10: Comparison of iron loss in the W1 part.

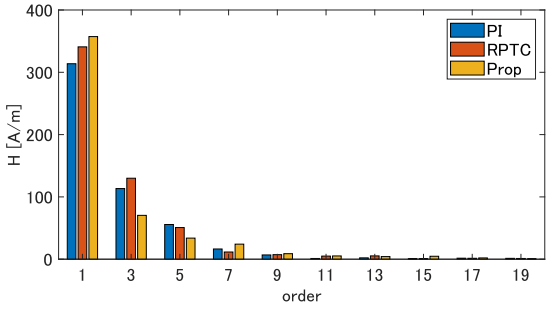

(a)

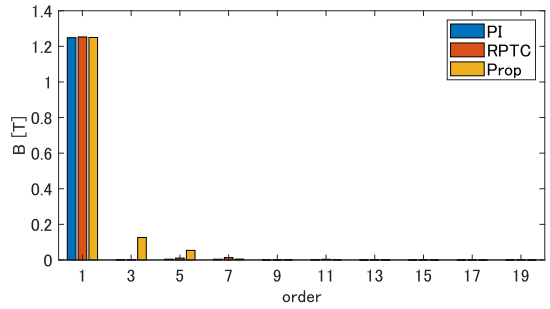

(b)

Fig. 11: Fourier transform results of of magnetic field strength and magnetic flux density. (a) magnetic field strength. (b) magnetic flux density.

10. The reductions were 21.9 % when RPTC was applied and 48.6% when the proposed method was applied compared to the PI control.

Fig. 11 shows the Fourier transform results of magnetic field strength and magnetic flux density. Fig. 11a and Fig. 11b represent the corresponding magnetic field strength and flux density, respectively.

In Fig. 11a, compared with the PI control, the third-order harmonic amplitude of the magnetic field strength increased in RPTC, and the phase of the third-order harmonic was nearly in phase with the fundamental wave, resulting in thinner hysteresis and reduced iron loss. On the other hand, in the proposed method, the third-order harmonic amplitude of the magnetic field strength was smaller, and the phase of the third-order and fifth-order components was opposite to the fundamental wave, while the seventh-order component was in phase with the fundamental wave, which suppressed the peak of magnetic field strength and was considered to significantly reduce iron loss.

In terms of the magnetic flux density results, Fig. 11b shows that the fundamental wave amplitudes of the magnetic flux density were the same for all methods, and that the magnetic flux density had almost no low-order harmonics when PI control was applied, and the low-order harmonics increased only slightly when RPTC was applied compared to PI control. However, when the proposed method was applied, the amplitude of the third-order harmonic was 0.12 T and that of the fifth-order harmmonic was 0.054 T, indicating an

TABLE IV: Losses measured by power meter.

Control method	Copper loss	Iron loss + Mechanical loss
PI	16.57 W	31.87 W
RPTC	16.53 W	31.46 W
Prop	17.20 W	33.23 W

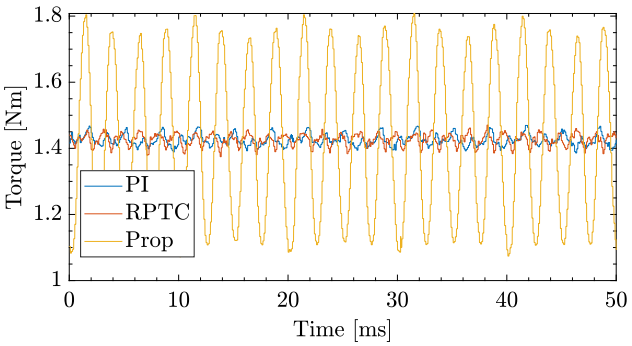

Fig. 12: Torque comparison for each control method.

increase compared to the PI control and RPTC cases. The third-order harmonic was in phase with the fundamental wave, and the fifth-order harmonic was opposite to the fundamental wave, which suppressed the peak and reduced the iron loss significantly.

Table IV shows the results of each loss for the entire motor as measured with a power meter. Copper losses and the sum of iron losses and mechanical losses are reduced in RPTC compared to PI control due to the suppression of current harmonics. However, both are found to have increased in the proposed method compared to the conventional method due to the injection of current harmonics. Fig. 12 shows the torque waveforms caluclated by measured dq-axis currents. The proposed method has generated more torque ripple than the conventional methods.

V. Conclusion

This paper compared and evaluated the iron loss generated in the W1 part of the teeth by three different current control methods: PI control, RPTC for low-order harmonic currents suppression, and proposed method, by H-coil method. As a result, RPTC and proposed method reduced iron loss in the W1 part by 21.9% and 48.6%, respectively compared with PI control. The reason for the reduced iron loss was further discussed based on the changes in the harmonics of the magnetic field strength and flux density. As a future study, a current control method to improve motor efficiency will be discussed, taking into account the increase of harmonic copper loss due to harmonic current injection.

References

[1] Ji-Hoon Jang, Jung-Ik Ha, M. Ohto, K. Ide and S. -K. Sul, "Analysis of permanent-magnet machine for sensorless control based on high-frequency signal injection," IEEE Transactions on Industry Applications, vol. 40, no. 6, pp. 1595-1604, 2004.

[2] M. D. Nardo et al., "Permanent Magnet Assisted Synchronous Reluctance Machine Design for Light Traction Applications," IEEE Transactions on Industry Applications, vol. 60, no. 4, pp. 6079-6091, 2024.

[3] J. Ohata, H. Haga, M. Konoto, and Q. Piao, "Reduction Method of Zero-Sequence Current in 6-Step Operation on One Side of Dual Inverter with a Common DC-Bus," IEEJ Journal of Industry Applications, vol. 13, no. 3, pp. 280-289, 2024.

[4] H. Matsumori, T. Kosaka, N. Matsui and S. Saha, "Alternative PWM Switching Strategy Implementation for a Dual Inverter Fed Open Winding Motor Drive System for an Electric Vehicle Application," IEEE Transactions on Industry Applications, vol. 59, no. 5, pp. 5957-5970, 2023.

[5] S. Rubino, O. Dordevic, E. Armando, I. R. Bojoi and E. Levi, "A Novel Matrix Transformation for Decoupled Control of Modular Multiphase PMSM Drives," IEEE Transactions on Power Electronics, vol. 36, no. 7, pp. 8088-8101, 2021.

[6] J. Yoo and S. -K. Sul, "Dynamic Overmodulation Scheme for Improved Current Regulation in PMSM Drives," IEEE Transactions on Power Electronics, vol. 37, no. 6, pp. 7132-7144, 2022.

[7] T. Inoue, Y. Inoue, S. Morimoto, and M. Sanada, "Maximum Torque per Ampere Control of a Direct Torque-Controlled PMSM in a Stator Flux Linkage Synchronous Frame," IEEE Transactions on Industry Applications, vol.52, no.3, pp.2360–2367, 2016.

[8] T. Kumagai, T. Ito, K. Nishikawa, J. Ito, K. Yamane, N. Yamada, and M. Niwa, "Reduction of Iron Loss in Stator Core using an Optinum Pulse Pattern for High-Speed IPMSM," IEEJ Transactions on Industry Applications, vol. 141-D, no. 4, pp.313-323, 2021. (in Japanese)

[9] K. Iwama, and T. Noguchi, "High-Efficiency Drive Method of Adjustable Field IPMSM Utilizing Magnetic Saturation," IEEE Access, vol.10, pp.1254999-125508, 2022.

[10] A. Balamurali, A. Kundu, Z. Li and N. C. Kar, "Improved Harmonic Iron Loss and Stator Current Vector Determination for Maximum Efficiency Control of PMSM in EV Applications," IEEE Transactions on Industry Applications, vol. 57, no. 1, pp. 363-373, 2021.

[11] H. Kim, Y. Han, K. Lee and S. Bhattacharya, "A Sinusoidal Current Control Strategy Based on Harmonic Voltage Injection for Harmonic Loss Reduction of PMSMs With NonSinusoidal Back-EMF," IEEE Transactions on Industry Applications, vol. 56, no. 6, pp.7032-7043, 2020.

[12] W. Liang, P. Chi-Kwong Luk, and W. Fei, "Investigation of magnetic field interharmonics and sideband vibration in the FSCW IPMSM drive with the SPWM technique," IEEE Transactions on Power Electronics, vol. 33, no. 4, pp. 3315–3324, 2018.

[13] N. G. M. Thao, L. T-That, K. Fujisaki, K. Naruse, and H. Naitoh, "Conceptual Diagrams of Extended Building Factor for Analysis and Evaluation of Factors on Core Loss Density Increase in IPMSM," IEEJ Journal of Industry Applications, vol. 12, no. 1, pp. 12-25, 2023.

[14] Y. Ito, and Y. Iwaji, "Harmonic Reduction Method Using Minor Sampling Process for Sensorless Signal Injection-Based Position Control Technique," IEEJ Journal of Industry Applications, vol. 12, no. 4, pp. 719-725, 2023.

[15] K. Okazaki, K. Yang, and K. Akatsu, "Real-time Dynamic Eccentricity Detection by Analyzing Harmonic Components of No-load Line-line Voltages in Multi-three-phase PMSMs," IEEJ Journal of Industry Applications, vol. 12, no. 3, pp. 409-417, 2023.

[16] F. Nishanth, A. Khamitov and E. L. Severson, "Design of Electric Machine Windings to Independently Control Multiple Airgap Harmonics," IEEE Transactions on Industry Applications, vol. 60, no. 2, pp. 3039-3050, 2024.

[17] Y. Inagaki, M. Mae, O. Shimizu, S. Nagai, H. Fujimoto, T. Miyajima, Y. Yasuda, and A. Yamagiwa, "Effect of Harmonic Current Suppression on Iron Loss of IPMSM Using Repetitive Perfect Tracking Control," IEEJ Journal of Industry Applications, vol. 11, no. 2, pp. 317-326, 2022.

[18] M. Nakagawa, "Development of Measurement Technique of Magnetic Steel Losses Excited by Inverter," Technology Research Association of Magnetic Materials for High-Efficiency Motors, pp. 57-67, 2022.(in Japanese)

[19] H. Fujimoto, Y. Hori, and A. Kawamura, "Perfect tracking control based on multirate feedforward control with generalized sampling periods," IEEE Transactions on Industrial Electronics, vol. 48, no. 3, pp. 636-644, 2001.

[20] K. K. Chew, and M. Tomizuka, "Digital Control of Repetitive Errors in Disk Drive Systems," IEEE Control Systems Magazine, vol. 10, no. 1, pp. 16–20, 1990.